Falling films on flexible inclines

O. K. Matar,[1,*] R. V. Craster,[2] and S. Kumar[3]
[1]*Department of Chemical Engineering, Imperial College London, South Kensington Campus, London, SW7 2AZ, United Kingdom*
[2]*Department of Mathematics, Imperial College London, South Kensington Campus, London, SW7 2AZ, United Kingdom*
[3]*Department of Chemical Engineering and Materials Science, University of Minnesota, Minneapolis, Minnesota 55455, USA*
(Received 28 July 2007; published 8 November 2007)

The nonlinear stability and dynamic behavior of falling fluid films is studied for flow over a flexible substrate. We use asymptotic methods to deduce governing equations valid in various limits. Long-wave theory is used to derive Benney-like coupled equations for the film thickness and substrate deflection. Weakly nonlinear equations are then derived from these equations that, in the limit of large wall damping and/or large wall tension, reduce to the Kuramoto-Sivashinsky equation. These models break down when inertia becomes more significant, so we also use a long-wave approximation in conjunction with integral theory to derive three strongly coupled nonlinear evolution equations for the film thickness, substrate deflection, and film volumetric flow rate valid at higher Reynolds numbers. These equations, accounting for inertia, capillary, viscous, wall tension, and damping effects, are solved over a wide range of parameters. Our results suggest that decreasing wall damping and/or wall tension can promote the development of chaos in the weakly nonlinear regime and lead to severe substrate deformations in the strongly nonlinear regime; these can give rise to situations in which the free surface and underlying substrate come into contact in finite time.

DOI: 10.1103/PhysRevE.76.056301 PACS number(s): 47.55.nb, 47.85.Dh, 47.20.Ma

I. INTRODUCTION

The dynamics of thin films have been well studied over the past decades due to their relevance to a variety of applications in industrial, biophysical, and daily life settings [1,2]. Films flowing down an incline under the action of gravity have received particular attention due to their importance in applications, for instance, in reaction engineering and distillation, and in the design of heat exchanger units for heating and cooling [3]. Early experimental work by Kapitza [4,5] and the more recent studies by Alekseenko *et al.* [6], Gollub *et al.* [7–9], Nosoko *et al.* [10–12], and Bontozoglou *et al.* [13,14] have demonstrated that this flow is accompanied by the development of large-amplitude waves. The work by Liu *et al.* [9] showed that the wave structure downstream of the inlet can be controlled via periodic forcing of the flow rate at the inlet and also demonstrated the existence of secondary instabilities, following the initial bifurcation from a flat-film steady state, that are responsible for transitions from two- to three-dimensional wave patterns.

Linear stability analyses of the waveless solution when gravitational forcing is balanced by viscous drag were carried out by Yih [15,16] and Benjamin [17] who showed this base state to be unstable to long-wavelength disturbances due to the presence of inertia. An evolution equation for the film thickness was then derived by Benney [18], which accounts for inertia, hydrostatic pressure, and capillary and viscous effects; this equation was then used to model the dynamics in the nonlinear regime. Falling film dynamics in the nonlinear regime have also been studied by a number of investigators [1,3,19–28]. In the Benney equation and in other equations derived using a similar approach, inertia enters the problem at order δ, which is the film aspect ratio, assumed to be small. Consequently, these equations cannot be used to model the film dynamics at moderate to large Reynolds numbers [23,29–33] often leading to finite-time "blow-up" of the solutions. Weakly nonlinear evolution equations such as the celebrated Kuramoto-Sivashinsky equation have also been derived (it is possible to do so from the Benney equation, for instance) [34–44]. The solutions of these equations remain bounded and can be periodic, quasiperiodic, or chaotic depending on the length of the spatial domain [39,45–50].

Complementary to this are approaches involving a combination of boundary-layer theory and an integral approximation that relies on the use of a semiparabolic profile as a closure relation for the film streamwise velocity distribution. This approach was pioneered by Kapitza [51] and Shkadov [52] and leads to a strongly coupled pair of nonlinear evolution equations for the film thickness and volumetric flow rate. These equations do not suffer from the blow-up problem and are valid at higher Reynolds numbers, but they do exhibit solution nonuniqueness [52–55]. Nevertheless, the attracting wave regimes or so-called "family" of "dominating waves," that have the largest velocity and maximal film thickness, compare favorably with experimental observations [52,56]. If the inclined plane is not vertical, there exists, however, a discrepancy between the predictions of the Shkadov and the Orr-Sommerfeld equations, the latter being obtained via the linearization of the Navier-Stokes equations. Agreement with the Orr-Sommerfeld equations is obtained by employing an adjustment to the Shkadov approach by using a weighted residual in which a semiparabolic velocity profile is used as a test function and the weighting function is the test function itself [31,33].

The studies cited in the brief review above have all been carried out for the case of a fluid film flowing over a rigid wall. The extension to falling films flowing over flexible substrates has, to our knowledge, not been considered previously. Situations where there is a strong coupling between

*o.matar@imperial.ac.uk

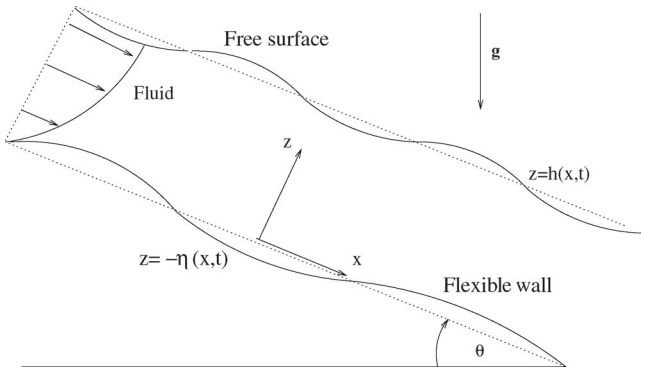

FIG. 1. Schematic representation of the flow geometry.

the flowing fluid and a flexible structure are of interest since this scenario arises in a wide range of settings; these include studying the delay in the transition to turbulence [57], modeling of airflow in pulmonary airways [58] and blood flow in the heart [59], the use of rubber-covered rolls to reduce defects in coating process [60], and instabilities near polymer interfaces [61]. More recently, Matar and Kumar showed that wall flexibility can have a considerable effect on the rupture of thin films [62] and can destabilize a ridge formed at the contact line in flow down an inclined plane [63]. It is therefore expected that the properties of a flexible wall will have a significant effect on the dynamics of a falling film. We aim to generate the appropriate governing equations, investigate the inter-relation between those that are derived in different limits, and determine whether the flexible substrate acts to damp out or exacerbate instabilities.

We first, in Sec. II C, use long-wave theory to derive a pair of coupled equations for the film thickness and wall deflection that represent an extension to the Benney equation. A pair of weakly nonlinear equations then emerge from this as an extension of the Kuramoto-Sivashinsky equation. We then use, in Sec. II D, a similar approach to that of Shkadov to derive three coupled equations for the film thickness and volumetric flow rate that are now coupled to wall deflection. Both these and the Benney-like equation emerge by taking different limits. In both cases the linear stability of the equations is examined (Sec. III) together with the behavior of the systems in the nonlinear regime (Sec. IV). The predictions of the three sets of equations are then compared and indicate that wall flexibility promotes film instability. The weakly nonlinear system exhibits chaotic solutions under certain conditions and the long-wave modified Benney system suffers from finite-time blow-up, which is absent in the modified Shkadov system. Some concluding remarks are given in Sec. V.

II. FORMULATION

A. Governing equations

We consider the dynamics of an incompressible Newtonian film of viscosity μ and density ρ overlying an infinitely long, flexible, impermeable substrate, inclined to the horizontal at an angle θ, as shown in Fig. 1. The film is bounded above by a gas, assumed to be inviscid. A rectangular coordinate system $(x,0,z)$ models the two-dimensional film dynamics, where x and z denote the streamwise and normal coordinates to the inclined substrate. The instantaneous locations of the gas-liquid and solid-liquid interfaces are $z=h(x,t)$ and $z=-\eta(x,t)$, respectively, while their undisturbed locations are at $z=h_0$ and $z=0$, respectively. The film flows under the action of gravity with a velocity field $\mathbf{u}=(u,0,v)$, in which u and v denote its streamwise and normal velocity components.

The film dynamics are governed by the continuity and Navier-Stokes equations

$$u_x + v_z = 0, \tag{1}$$

$$u_t + uu_x + vu_z = -\frac{p_x}{\rho} + \nu(u_{xx} + u_{zz}) + g\sin\theta, \tag{2}$$

$$v_t + uv_x + vv_z = -\frac{p_z}{\rho} + \nu(v_{xx} + v_{zz}) - g\cos\theta, \tag{3}$$

where p denotes pressure, g the gravitational acceleration, and ν the kinematic viscosity; the subscripts x, z, and t denote partial differentiation with respect to x, z, and time t.

The substrate dynamics are governed by a forced membrane equation

$$\rho_w h_w \gamma \eta_t - \frac{T}{(1+\eta_x^2)^{1/2}}\eta_{xx} = (1+\eta_x^2)(p - p_w) + 2\mu[\eta_x(u_z + v_x) - (v_z + \eta_x^2 u_x)], \tag{4}$$

which is the simplest system that couples a restoring force with the normal force imposed by the fluid. Similar models have been used in prior work [62–65]. Here ρ_w, h_w, and γ denote the substrate density, thickness, and damping coefficient, respectively, and p_w represents the pressure external to the wall. We have also assumed the substrate to be isotropic and sufficiently thin for its tension T to remain uniform across its thickness; it is tethered at one end so that the amplitude of deflections normal to its axis far exceed that of longitudinal deformations. Under these conditions, bending stresses can be neglected [66,67].

Solutions of the above governing equations are subject to the following boundary conditions

$$u = 0, \quad \eta_t = -v, \quad \text{at} \quad z = -\eta, \tag{5}$$

corresponding to no-slip and continuity of velocity. At the upper interface, $z=h$, the kinematic boundary condition and the tangential stress and normal stress conditions are

$$h_t + uh_x = v, \tag{6}$$

$$(1-h_x^2)(u_z + v_x) + 4h_x v_z = 0, \tag{7}$$

$$p_g - p + 2\mu\frac{(1+h_x^2)}{(1-h_x^2)}v_z = \sigma\frac{h_{xx}}{(1+h_x^2)^{3/2}}, \tag{8}$$

in which p_g denotes the pressure of the gas above the film and σ represents the (constant) surface tension of the gas-

liquid interface. Here, we have made use of continuity in expressing Eq. (7), which, in turn, was used to obtain Eq. (8). Equations (1)–(4) admit steady solutions satisfying the boundary conditions given by Eqs. (5)–(8): $\bar{h}=h_0$, $\bar{\eta}=0$, $\bar{v}=0$,

$$\bar{u}=\frac{g\sin\theta}{2\nu}z(2h_0-z),$$

$$\bar{p}=p_g+\rho g(h_0-z)\cos\theta, \tag{9}$$

and $p_w=p_0+\rho g h_0\cos\theta$.

B. Scaling

The governing equations and boundary conditions are rendered dimensionless using a scaling based on the equilibrium film thickness h_0

$$(x,z,h,\eta)=h_0(\tilde{x},\tilde{z},\tilde{h},\tilde{\eta}),\quad (u,v)=U(\tilde{u},\tilde{v}),$$

$$t=(h_0/U)\tilde{t},\quad p=\rho U^2\tilde{p}, \tag{10}$$

and the representative velocity scale $U\equiv\bar{u}(z=h_0)=g\sin\theta h_0^2/2\nu$ that is the steady surface velocity; here, the tildes, which are subsequently suppressed, denote dimensionless quantities. The dimensionless Navier-Stokes equations are then given by

$$u_t+uu_x+vu_z=-p_x+\frac{1}{\mathrm{Re}}(u_{xx}+u_{zz})+\frac{2}{\mathrm{Re}}, \tag{11}$$

$$v_t+uv_x+vv_z=-p_z+\frac{1}{\mathrm{Re}}(v_{xx}+v_{zz})-\frac{2}{\mathrm{Re}}\cot\theta, \tag{12}$$

where $\mathrm{Re}\equiv Uh_0/\nu$ is the Reynolds number; the continuity equation remains unaltered from Eq. (1). The dimensionless version of Eq. (4) is expressed by

$$B\eta_t-\frac{1}{C_w}\frac{\eta_{xx}}{(1+\eta_x^2)^{1/2}}=\mathrm{Re}(p-p_w)(1+\eta_x^2)+2[\eta_x(u_z+v_x)-v_z(1-\eta_x^2)], \tag{13}$$

where $B\equiv\rho_w h_w\gamma h_0/\mu$ provides a dimensionless measure of wall damping effects, $C_w\equiv\mu U/T$ is a wall capillary number and $p_w=p_g+(2/\mathrm{Re})\cot\theta$. Note that B can be rewritten as $B=(\rho_w h_w/\rho h_0)(\rho\gamma h_0^2/\mu)$, which is revealing as it is the product of the ratio of wall to fluid mass and that of wall to fluid damping. Wall inertia is assumed to be negligible relative to wall damping, and that corresponds to the limit $g\sin\theta h_0/\gamma\nu\ll 1$.

The dimensionless boundary conditions at $z=h(x,t)$ are expressed by

$$h_t+uh_x=v, \tag{14}$$

$$(1-h_x^2)(u_z+v_x)+4h_x v_z=0, \tag{15}$$

$$\frac{\mathrm{Re}}{2}(p_g-p)+\frac{(1+h_x^2)}{(1-h_x^2)}v_z=\frac{1}{2C}\frac{h_{xx}}{(1+h_x^2)^{3/2}}, \tag{16}$$

where $C\equiv\mu U/\sigma$ is a capillary number. The boundary conditions at $z=-\eta(x,t)$ remain unaltered. The dimensionless steady solutions are

$$\bar{h}=1,\quad \bar{\eta}=0,\quad \bar{u}=z(2-z),\quad \bar{v}=0,$$

$$\bar{p}=p_g+\frac{2}{\mathrm{Re}}\cot\theta(1-z). \tag{17}$$

We aim to model the dynamics of long waves. We therefore introduce the following rescalings:

$$x=\frac{\xi}{\delta},\quad t=\frac{\tau}{\delta},\quad v=\delta w, \tag{18}$$

into the above dimensionless governing equations and boundary conditions. Here, $\delta\equiv h_0/\Lambda\ll 1$ in which Λ represents the wavelength of a typical coherent wavy structure and thus provides a lateral lengthscale. These rescalings yield

$$\delta(u_\tau+uu_\xi+wu_z)=-\delta p_\xi+\frac{1}{\mathrm{Re}}(u_{zz}+\delta^2u_{\xi\xi})+\frac{2}{\mathrm{Re}}, \tag{19}$$

$$\delta^2(w_\tau+uw_\xi+ww_z)=-p_z+\frac{\delta}{\mathrm{Re}}(w_{zz}+\delta^2w_{\xi\xi})-\frac{2}{\mathrm{Re}}\cot\theta, \tag{20}$$

$$u_\xi+w_z=0, \tag{21}$$

which then have both δ and Re within them. These equations couple to those of the flexible substrate and upper interface via

$$\delta B\eta_\tau-\frac{\delta^2}{C_w}\frac{\eta_{\xi\xi}}{\Delta_w}=\mathrm{Re}(1+\delta^2\eta_\xi^2)(p|_{-\eta}-p_w)+2\delta(\eta_\xi[u_z+\delta^2w_\xi]-w_z[1-\delta^2\eta_\xi^2])|_{-\eta}, \tag{22}$$

$$u|_{-\eta}=0,\quad \eta_\tau=-w|_{-\eta}, \tag{23}$$

$$h_\tau+u|_h h_\xi=w|_h, \tag{24}$$

$$(1-\delta^2h_\xi^2)(u_z+\delta^2w_\xi)|_h+4\delta^2h_\xi w_z|_h=0, \tag{25}$$

$$\frac{\mathrm{Re}}{2}(p_g-p|_h)+\delta\left(\frac{1+\delta^2h_\xi^2}{1-\delta^2h_\xi^2}\right)w_z|_h=\frac{\delta^2}{2C}\frac{h_{\xi\xi}}{(1+\delta^2h_\xi^2)^{3/2}}. \tag{26}$$

These equations, in turn, involve both δ and the dimensionless groups associated with substrate flexibility B and C_w, and capillary effects C. We focus below on two distinguished limits $\mathrm{Re}=O(1)$ and $\mathrm{Re}=O(\delta^{-1})$, that correspond to low and moderate Reynolds numbers, respectively. In both cases, nonlinear equations emerge, and we are interested in exploring their behavior and inter-relation.

C. Re=$O(1)$: Long-wave theory

We introduce the following decomposition for u, v, and p into Eqs. (19)–(26):

$$(u,v,p) = (\bar{u},\bar{v},\bar{p}) + (\hat{u},\hat{v},\hat{p}), \tag{27}$$

along with the following expansions for $(\hat{u},\hat{v},\hat{p},h,\eta)$:

$$(\hat{u},\hat{v},\hat{p},h,\eta) = (u_0,w_0,p_0,H_0,\eta_0) + \delta(u_1,w_1,p_1,H_1,\eta_1). \tag{28}$$

To ensure that capillary, wall tension and damping effects are retained in the leading-order dynamics we also rescale C, C_w, and B:

$$C = \delta^2\hat{C}, \quad C_w = \delta^2\hat{C}_w, \quad B = \frac{\hat{B}}{\delta}, \tag{29}$$

where $(\hat{C},\hat{C}_w,\hat{B})=O(1)$. This yields a hierarchy of problems that are solved order by order in powers of δ.

1. Leading-order equations

Substituting the expansion into the governing equations and boundary conditions gives a system of equations that is readily solved to give the leading order velocity components and pressure as

$$u_0 = 2(H_0-1)(z+\eta_0) + \eta_0(2+\eta_0), \tag{30}$$

$$w_0 = -\eta_{0\tau} - 2(\eta_0+H_0)_\xi(\eta_0+H_0)(z+\eta_0) + H_{0\xi}[(H_0+\eta_0)^2 - (H_0-z)^2], \tag{31}$$

$$p_0 = -\frac{2}{\mathrm{Re}}\left[\cos\theta(1-H_0) + \frac{1}{2\hat{C}}H_{0\xi\xi}\right], \tag{32}$$

and the following coupled evolution equations for the leading order height H_0 and substrate deflection η_0:

$$H_{0\tau} + \eta_{0\tau} + 2(\eta_0+H_0)^2(\eta_0+H_0)_\xi = 0, \tag{33}$$

$$\hat{B}\eta_{0\tau} - \frac{\eta_{0\xi\xi}}{\hat{C}_w} + \frac{H_{0\xi\xi}}{\hat{C}} + 2\cos\theta[1-(\eta_0+H_0)] = 0. \tag{34}$$

2. The $O(\delta)$ equations

The relevant equations at $O(\delta)$ are given by

$$u_{0\tau} + (\bar{u}+u_0)u_{0\xi} + w_0(\bar{u}_z+u_{0z}) = -p_{0\xi} + \frac{u_{1zz}}{\mathrm{Re}},$$

$$p_{1z} = \frac{1}{\mathrm{Re}}w_{0zz}, \quad u_{1\xi} + w_{1z} = 0, \tag{35}$$

$$\hat{B}\eta_{1\tau} - \frac{1}{\hat{C}_w}\eta_{1\xi\xi} = 2\cot\theta\eta_1 + 2\left[\eta_{0\xi}\left(2(1+\eta_0) + u_{0z}\big|_{-\eta_0}\right) - w_{0z}\big|_{-\eta_0}\right] + \mathrm{Re}\left(p_1\big|_{-\eta_0}\right), \tag{36}$$

$$u_1\big|_{-\eta_0} = 2(1+\eta_0)\eta_1 + 2(H_0-1)\eta_1,$$

$$\eta_{1\tau} = -w_1\big|_{-\eta_0} + w_{0z}\big|_{-\eta_0}\eta_1, \tag{37}$$

$$H_{1\tau} + [(\bar{u}_z+u_{0z})H_1 + u_1]\big|_{H_0}H_{0\xi} + (\bar{u}+u_0)\big|_{H_0}H_{1\xi} = w_1\big|_{H_0} + w_{0z}\big|_{H_0}H_1, \tag{38}$$

$$u_{1z}\big|_{H_0} = -\bar{u}_{zz}\big|_{H_0}H_1, \tag{39}$$

$$\cot\theta H_1 + w_1\big|_{H_0}w_{0z}\big|_{H_0} - \frac{\mathrm{Re}}{2}(p_1\big|_{H_0} + H_1p_{0z}\big|_{H_0}) = \frac{H_{1\xi\xi}}{2\hat{C}}. \tag{40}$$

Here $u_1|_{H_0}$, $w_1|_{H_0}$, $p_1|_{H_0}$, and $p_1|_{-\eta_0}$ are given by

$$u_1\big|_{H_0} = 2(\eta_0+H_0)(\eta_1+H_1) + \frac{5\,\mathrm{Re}}{6}(\eta_0+H_0)^5(\eta_0+H_0)_\xi - \frac{\mathrm{Re}}{2}(\eta_0+H_0)^2p_{0\xi}, \tag{41}$$

$$w_1\big|_{H_0} = -\eta_{1\tau} - (\eta_0+H_0)[2(2\eta_1+H_1)\eta_{0\xi} + 2\eta_1H_{0\xi} + (\eta_0+H_0)(H_{1\xi}+2\eta_{1\xi})] - \frac{\mathrm{Re}}{30}(\eta_0+H_0)^5(\eta_0+H_0)_\xi \times(96\eta_{0\xi}+71H_{0\xi}) + \frac{\mathrm{Re}}{2}(\eta_0+H_0)^2(2\eta_{0\xi}+H_{0\xi})p_{0\xi} - \frac{8\,\mathrm{Re}}{15}(\eta_0+H_0)^6(\eta_0+H_0)_{\xi\xi} + \frac{\mathrm{Re}}{3}(\eta_0+H_0)^3p_{0\xi\xi}, \tag{42}$$

$$p_1\big|_{H_0} = -\frac{2}{\mathrm{Re}}\left[-\cos\theta H_1 + 2(H_0+\eta_0)_\xi(\eta_0+H_0) + \frac{1}{2\hat{C}}H_{1\xi\xi}\right], \tag{43}$$

$$p_1\big|_{-\eta_0} = -\frac{2}{\mathrm{Re}}\left[-\cos\theta H_1 + 2(H_0+\eta_0)_\xi(\eta_0+H_0) + \frac{1}{2\hat{C}}H_{1\xi\xi} - H_{0\xi}(H_0+\eta_0)\right]. \tag{44}$$

Note that in the absence of wall deflections $(\eta_0,\eta_1)\to 0$, we obtain

$$u_1\big|_{H_0} = -\frac{\mathrm{Re}}{2}H_0^2p_{0\xi} + \frac{5\,\mathrm{Re}}{6}H_0^5H_{0\xi} + 2H_0H_1,$$

$$w_1\big|_{H_0} = \frac{\mathrm{Re}}{3}H_0^3p_{0\xi\xi} + \frac{\mathrm{Re}}{2}H_0^2H_{0\xi}p_{0\xi} - \frac{71\,\mathrm{Re}}{30}H_0^5H_{0\xi}^2 - \frac{8\,\mathrm{Re}}{15}H_0^6H_{0\xi\xi} - H_0^2H_{1\xi}, \tag{45}$$

where p_0 is given by Eq. (32), which agree with the expres-

sions obtained by Benney for the disturbance velocity components [18,44]. Notably in this limit, p_1 is not required.

Evolution equations for the film thickness and substrate deflection can be obtained, correct to $O(\delta)$, by adding Eq. (33) to δ multiplied by Eq. (38), and adding Eq. (34) to δ multiplied by Eq. (36):

$$d_\tau + \left[\frac{2}{3}d^3 + \delta\left(\frac{8\,\mathrm{Re}}{15}d^6 d_\xi - \frac{2}{3}\cot\theta d^3 H_\xi\right) + \frac{\delta}{3\hat{C}}d^3 H_{\xi\xi\xi}\right]_\xi = 0, \tag{46}$$

$$\hat{B}\eta_\tau - 2(d-1)\cos\theta - \frac{1}{\hat{C}_w}\eta_{\xi\xi} + \frac{1}{\hat{C}}H_{\xi\xi} - 2\delta d(2\eta - H)_\xi = 0, \tag{47}$$

where $d=H+\eta=(H_0+\delta H_1)+(\eta_0+\delta\eta_1)$. Equations (46) and (47) are therefore the natural extension of the Benney equation to account for substrate deflection in addition to inertia, viscous retardation, and capillarity. It is anticipated that these equations will suffer from the same problems as those that plague the Benney equation, that is, the occurrence of finite-time blow-up, where the assumptions underlying this equation become invalid.

3. Weakly nonlinear evolution equations

Here, we focus on $\theta=\pi/2$; indeed we shall for clarity use $\theta=\pi/2$ henceforth unless stated otherwise, i.e., a vertical wall. The weakly nonlinear limit is of interest for the onset of instability and as an accessible model that shows how nonlinearity affects the flow. We introduce the following forms for H and η: $H=1+\delta\tilde{H}$ and $\eta=\delta\tilde{\eta}$, into the Benney-like equations. Substitution of this expansion into Eq. (46) yields

$$\tilde{d}_\tau + 2\tilde{d}_\xi + 4\delta\tilde{d}\tilde{d}_\xi + \delta\left(\frac{8\,\mathrm{Re}}{15}\tilde{d}_{\xi\xi} + \frac{1}{3\hat{C}}\tilde{H}_{\xi\xi\xi\xi}\right) = 0 + O(\delta^2). \tag{48}$$

It is convenient to remove the linear first derivative term by moving to a moving coordinate $\tilde{\xi}=\xi-2\tilde{\tau}/\delta$, which results in the following equation for $\tilde{d}$:

$$\tilde{d}_{\tilde{\tau}} + 4\tilde{d}\tilde{d}_{\tilde{\xi}} + \frac{8\,\mathrm{Re}}{15}\tilde{d}_{\tilde{\xi}\tilde{\xi}} + \frac{1}{3\hat{C}}\tilde{H}_{\tilde{\xi}\tilde{\xi}\tilde{\xi}\tilde{\xi}} = 0. \tag{49}$$

Introduction of the rescalings $\tilde{\tau}=a_1 t$, $\tilde{\xi}=a_2 x$, and $(\tilde{d},\tilde{H},\tilde{\eta})=a_3(d,H,\eta)$, where a_1, a_2, and a_3 are given by

$$a_1 = \frac{75}{64\,\mathrm{Re}^2\hat{C}}, \quad a_2 = \left(\frac{5}{8\,\mathrm{Re}\,\hat{C}}\right)^{1/2}, \quad a_3 = \left[\left(\frac{2\mathrm{Re}}{15}\right)^3\hat{C}\right]^{1/2}, \tag{50}$$

finally yields the fluid depth equation in its canonical form

$$d_t + dd_x + d_{xx} + H_{xxxx} = 0. \tag{51}$$

Repeating the above procedure for Eq. (47) leads to

$$\alpha\eta_x + \beta\eta_{xx} - H_{xx} = 0, \tag{52}$$

where $\alpha\equiv(5\hat{B}^2\hat{C}/2\,\mathrm{Re})^{1/2}$ and $\beta\equiv\hat{C}/\hat{C}_w$ and the elastic effects are now encapsulated in just two controlling parameters. Equations (51) and (52) are an extension of the Kuramoto-Sivashinsky equation allowing for a flexible substrate. The parameter α represents a ratio of wall damping, inertial and surface tension forces, and β is a ratio of wall and surface tension. Below, increasing α and β will be interpreted as an increase in wall damping and wall tension, respectively.

It is also possible to obtain a relation between η and H by first integrating Eq. (52) once to obtain $\eta_x+(\alpha/\beta)\eta=H_x/\beta+c_1(t)$, and recasting this as $[e^{(\alpha/\beta)x}\eta]_x=e^{(\alpha/\beta)x}(H_x/\beta+c_1)$; integration of this result leads to

$$\eta = \frac{\beta}{\alpha}c_1(t) + e^{-(\alpha/\beta)x}c_2(t) + \frac{1}{\beta}(H - H|_{x=0}e^{-(\alpha/\beta)x}) - \frac{\alpha}{\beta^2}e^{-(\alpha/\beta)x}\int_0^x e^{(\alpha/\beta)x'}H dx'. \tag{53}$$

Using periodicity (with period 2π), the following relations for the time-dependent functions c_1 and c_2 are obtained:

$$c_1(t) = \frac{\alpha}{\beta}[\eta|_{x=0} - c_2(t)], \tag{54}$$

$$c_2(t) = \frac{-\frac{\alpha}{\beta^2}e^{-2\pi\alpha/\beta}\int_0^{2\pi} e^{(\alpha/\beta)x'}H dx' + \frac{H|_{x=0}}{\beta}(1-e^{-2\pi\alpha/\beta})}{1-e^{-2\pi\alpha/\beta}}. \tag{55}$$

As a result, the following expression can be obtained for η:

$$\eta = \eta|_{x=0} + \frac{1}{\beta}(H - H|_{x=0}e^{-(\alpha/\beta)x}) - \frac{\alpha}{\beta^2}e^{-(\alpha/\beta)x}\int_0^x e^{(\alpha/\beta)x'}H dx' + c_2(t)(e^{-(\alpha/\beta)x} - 1). \tag{56}$$

D. Re=$O(\delta^{-1})$: Integral theory

We now turn our attention to a different limit, where the Reynolds number is larger and so we set $\mathrm{Re}=\delta^{-1}\widehat{\mathrm{Re}}$. In order to retain the effects of substrate flexibility and capillarity at leading order, we rescale C, C_w, and B as follows:

$$C = \delta^3\hat{C}, \quad C_w = \delta^3\hat{C}_w, \quad B = \frac{\hat{B}}{\delta^2}. \tag{57}$$

Substitution of these rescalings into Eqs. (19)–(26) yields

$$u_\tau + uu_\xi + wu_z = -p_\xi + \frac{1}{\widehat{\mathrm{Re}}}(u_{zz}+2) + O(\delta^2), \quad p_z = 0,$$

$$u_\xi + w_z = 0, \tag{58}$$

$$\hat{B}\eta_\tau - \frac{1}{\hat{C}_w}\eta_{\xi\xi\xi} = \widehat{\mathrm{Re}}(p|_{-\eta} - p_w) + O(\delta^2), \tag{59}$$

with boundary conditions

$$u|_{-\eta} = 0, \quad \eta_\tau = -\,w|_{-\eta}, \tag{60}$$

$$h_\tau + u|_h h_\xi = w|_h, \quad u_z|_h = 0, \quad p = p_g - \frac{1}{\widehat{\mathrm{We}}}h_{\xi\xi}, \tag{61}$$

where $\widehat{\mathrm{We}} \equiv \widehat{\mathrm{Re}}\,\hat{C}$ is a Weber number. Since $p_z = 0$, the pressure is given by

$$p = p_g - \frac{1}{\widehat{We}}h_{\xi\xi}, \tag{62}$$

whence the substrate deflection evolution equation is given by

$$\hat{B}\eta_\tau - \frac{\eta_{\xi\xi}}{\hat{C}_w} = \widehat{\mathrm{Re}}\left(\Delta p - \frac{h_{\xi\xi}}{\widehat{\mathrm{We}}}\right), \tag{63}$$

where $\Delta p \equiv p_g - p_w$.

Integration of the x component of the Navier-Stokes equations from $z=-\eta$ to $z=h$ and making use of the Leibniz rule, the continuity equation, the kinematic conditions at the gas-liquid and liquid-solid interfaces, and the no-slip condition yields

$$q_\tau + \left(\int_{-\eta}^{h} u^2 dz\right)_\xi = \frac{1}{\widehat{\mathrm{We}}}(h+\eta)h_{\xi\xi\xi} + \frac{1}{\widehat{\mathrm{Re}}}[-u_z|_{-\eta} + 2(h+\eta)], \tag{64}$$

where $q \equiv \int_{-\eta}^{h} u dz$ is the volumetric flow rate. Integration of the continuity equation and making use, once again, of the kinematic conditions at both interfaces and the no-slip condition yields

$$h_\tau + q_\xi + \frac{1}{\hat{B}}\left(\widehat{\mathrm{Re}}\,\Delta p + \frac{\eta_{\xi\xi}}{\hat{C}_w} - \frac{h_{\xi\xi}}{\hat{C}}\right) = 0. \tag{65}$$

At this point, we choose the following closure for u, which satisfies the no-slip and no-stress conditions at the liquid-solid and gas-liquid interfaces, respectively:

$$u = -\frac{3q}{2(h+\eta)^3}(z+\eta)(z-\eta-2h). \tag{66}$$

Substitution of this equation into Eq. (64) yields the following evolution equation for q:

$$q_\tau + \frac{6}{5}\left(\frac{q^2}{h+\eta}\right)_\xi = \frac{1}{\widehat{\mathrm{We}}}(h+\eta)h_{\xi\xi\xi} + \frac{1}{\widehat{\mathrm{Re}}}\left[2(h+\eta) - \frac{3q}{(h+\eta)^2}\right], \tag{67}$$

which is coupled to Eqs. (63) and (65). These three coupled equations then incorporate the effect of wall flexibility and are valid at higher Reynolds numbers than the Benney-like equations (46) and (47).

E. Limiting cases

We have derived two basic systems of evolution equations: the Benney-like equations, given by Eqs. (46) and (47), with their weakly nonlinear reduction, and the higher Reynolds number system, Eqs. (63), (65), and (67). Here, we examine a number of limiting cases of interest and demonstrate the interconnections between these different models. We first consider equations from the weakly nonlinear limit given by Eqs. (51) and (52). For $\alpha \gg 1$ and $\beta = O(1)$, $\eta \to 0$ and Eq. (51) reduces to

$$H_t + HH_x + H_{xx} + H_{xxxx} = 0, \tag{68}$$

which is the Kuramoto-Sivashinsky equation. A similar result follows for $\beta \gg 1$. The limits $(\alpha, \beta) \to \infty$ correspond to large wall damping rates and wall tension, and naturally recover the rigid wall case.

For $\alpha \ll 1$ and $\beta = O(1)$, we substitute the following uniform expansion in powers of α, $(H, \eta) = (H_0, \eta_0) + \alpha(H_1, \eta_1) + \cdots$, into Eqs. (51) [or Eq. (56)] and (52). To leading order in α, we get the following equations:

$$\eta_0 = (\hat{\beta} - 1)(H_0 - 1), \tag{69}$$

$$\hat{\beta}H_{0t} + \hat{\beta}[\hat{\beta}(H_0 - 1) + 1]H_{0x} + \hat{\beta}H_{0xx} + H_{0xxxx} = 0, \tag{70}$$

which is a modified Kuramoto-Sivashinsky equation, where $\hat{\beta} = 1 + 1/\beta$. Here η_0 is enslaved to Eq. (70) and physically this limit corresponds to weak wall damping, but comparable wall and surface capillary numbers. In the limit of low wall tensions $\beta \ll 1$ and $\alpha = O(1)$, an expansion in β can be performed, but further expansion in α reveals that this leads to an ill-posed equation so we do not consider it further.

In summary, if $\alpha \gg 1$ or $\beta \gg 1$ then $\eta = 0$ and the Kuramoto-Sivashinsky equation is recovered. If $\alpha \ll 1$ and $\beta = O(1)$ then the dynamics are described by Eqs. (69) and (70), while the $\beta \ll 1$ and $\alpha = O(1)$ case is governed by

$$\eta_0 = \frac{H_{0x}}{\alpha}, \tag{71}$$

$$d_{0t} + d_0 d_{0x} + d_{0xx} + H_{0xxxx} = 0; \tag{72}$$

the $(\alpha, \beta) \ll 1$ case is described by ill-posed equations and will not be considered further.

Equations (46) and (47) can also be simplified for $\hat{B} \gg 1$, or $\hat{C}_w \ll 1$, which correspond to high wall damping and tension, respectively, $\eta = 0$ and H is described by

$$H_t + \left[\frac{2}{3}H^3 + \delta\left(\frac{8}{15}\,\mathrm{Re}\,H^6 H_\xi + \frac{1}{3\hat{C}}H^3 H_{\xi\xi\xi}\right)\right]_\xi = 0, \tag{73}$$

which is the Benney equation as one would deduce for flow over a rigid wall.

It is also possible to reduce the higher Reynolds number equation system, Eqs. (63), (65), and (67), to those for $\mathrm{Re} \sim O(1)$, Eqs. (46) and (47). We set $p_g = p_w$ so that $\Delta p = 0$, rescale as follows:

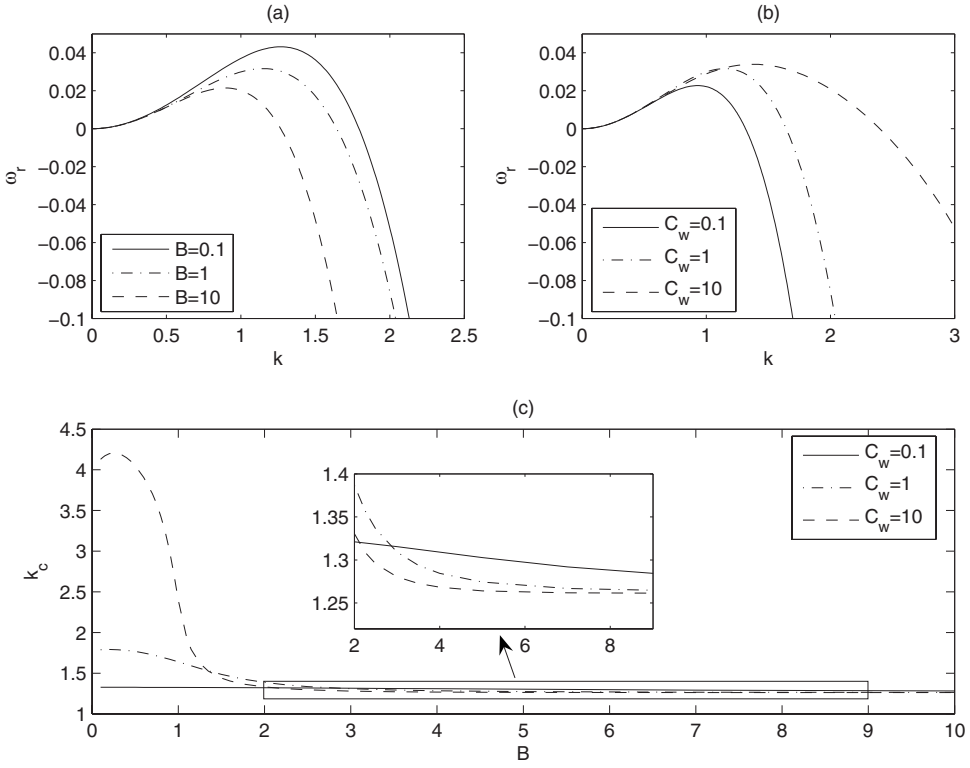

FIG. 2. Dispersion curves showing the effect of varying $\hat{B}$ (a) and $\hat{C}_w$ (b) on the linear stability of the falling film; (c) marginal stability curve. Unless stated otherwise in the legends, $\hat{B}=\widehat{\mathrm{Re}}=\widehat{\mathrm{We}}=\hat{C}=\hat{C}_w=1$.

$$\widehat{\mathrm{Re}}=\delta\widetilde{\mathrm{Re}},\quad \hat{C}=\frac{\tilde{C}}{\delta},\quad \hat{C}_w=\frac{\tilde{C}_w}{\delta},\quad \hat{B}=\delta\tilde{B}, \tag{74}$$

and expand uniformly in powers of δ: $(h,\eta,q)=(h_0,\eta_0,q_0)+\delta(h_1,\eta_1,q_1)+\cdots$. Substitution of this expansion and the above rescalings into Eq. (67) results in leading-order and first-order evolution equations; adding the leading-order ones to δ times the first-order ones gives

$$d_\tau+\left[\frac{2}{3}d^3+\frac{4\delta}{9}\widetilde{\mathrm{Re}}\,d^6d_\xi+\frac{\delta}{3\tilde{C}}d^3H_{\xi\xi\xi}\right]_\xi=0, \tag{75}$$

$$\tilde{B}\eta_\tau-\frac{\eta_{\xi\xi}}{\tilde{C}_w}+\frac{H_{\xi\xi}}{\tilde{C}}=0, \tag{76}$$

where $d=(h_0+\eta_0)+\delta(h_1+\eta_1)=H+\eta$. Thus one observes that Eq. (75) agrees with Eq. (46) except for the factor preceding the inertial term; this is due to the fact that the latter equation was derived using a formal perturbation expansion whilst Eqs. (63), (65), and (67) were obtained by postulating a closure relation for the streamwise velocity distribution. The discrepancy between Eqs. (47) and (76), which arises at $O(\delta)$, is due to the procedure used to derive Eq. (47) and allows the perturbation pressure to depend on the leading order vertical component of velocity $p_{1z}=w_{0zz}/\mathrm{Re}$; such a dependence is absent in the case of Eq. (76).

Finally, for $\hat{B}\gg 1$ or $\hat{C}_w\ll 1$, Eq. (63) gives $\eta=0$ and Eqs. (65) and (67) reduce to

$$h_t+q_\xi=0,$$

$$q_\tau+\frac{6}{5}\left(\frac{q^2}{h}\right)_\xi=\frac{1}{\widehat{\mathrm{We}}}hh_{\xi\xi\xi}+\frac{1}{\widehat{\mathrm{Re}}}\left[2h-\frac{3q}{h^2}\right], \tag{77}$$

which are the Shkadov equations (except for rescalings).

III. LINEAR STABILITY ANALYSIS

Here, we present results of a linear stability analysis of the various models derived in the previous section to describe the dynamics of falling films on flexible substrates.

A. Long-wave theory

We perturb Eqs. (46) and (47) as follows:

$$(d,\eta)=(1,0)+(\hat{d},\hat{\eta})e^{ikx}e^{\lambda t}, \tag{78}$$

and linearize the resultant equations to obtain the following characteristic equation for the complex growth rate λ as a function of the (real) wave number k and the relevant system parameters

$$\left(\hat{B}\lambda+\frac{k^2}{\hat{C}_w}+4ik\delta\right)\left(\lambda+2ik-\frac{8\,\mathrm{Re}}{15}\delta k^2+\delta\frac{k^4}{3\hat{C}}\right)+\left(\lambda+2ik-\frac{8\,\mathrm{Re}}{15}\delta k^2\right)\left(2ik\delta+\frac{k^2}{\hat{C}}\right)=0. \tag{79}$$

The marginal stability curve is obtained by setting $\lambda_r=0$ which yields a relation between k_c, the "cutoff" wave number beyond which $\lambda_r<0$, and system parameters; this is shown in Fig. 2 along with dispersion curves, which depict the dependence of λ_r on k. Inspection of Fig. 2 reveals that for $\hat{B}<1$, that is, for relatively weak wall damping, decreasing the

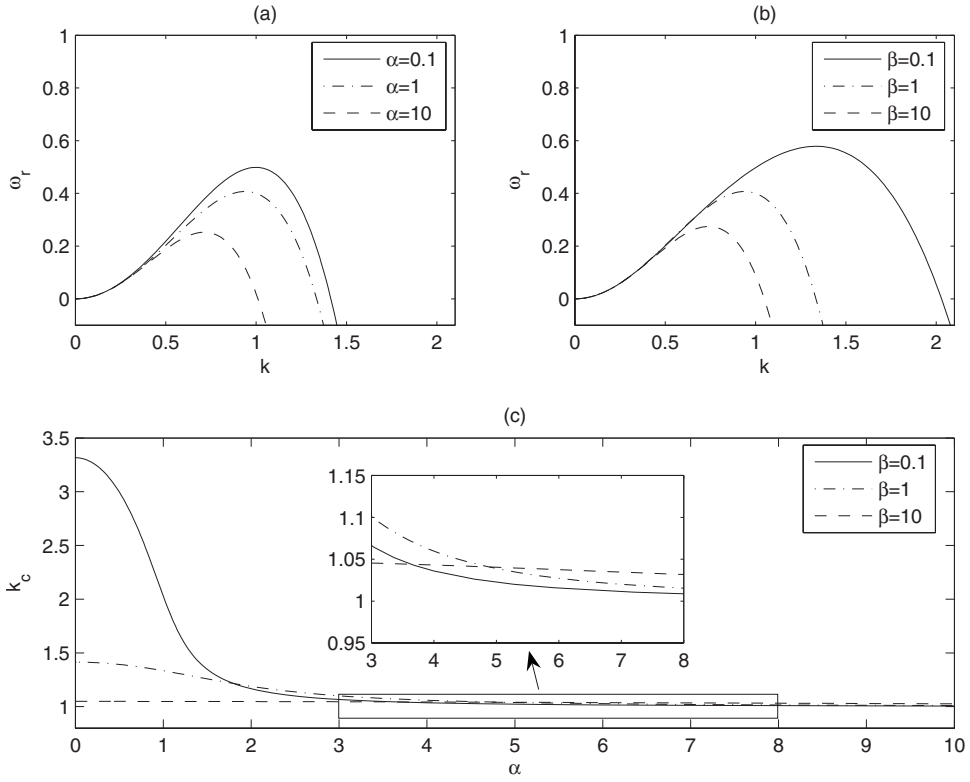

FIG. 3. Dispersion curves showing the effect of varying α (a) and β (b) on the linear stability of the falling film; (c) marginal stability curve. Unless stated otherwise in the legends, $\alpha=\beta=1$.

magnitude of wall tension by increasing $\hat{C}_w$ is destabilizing leading to a large increase in k_c. For larger values of $\hat{B}$, however, k_c increases with wall tension, as shown in the inset in Fig. 2; this trend reversal occurs for a value of $\hat{B}$ close to unity. For a given value of $\hat{C}_w$, k_c exhibits an overall decreasing trend with increasing $\hat{B}$ and, for weak wall tension, k_c has a maximum for small $\hat{B}$ and a shallow minimum at intermediate $\hat{B}$ values.

In Fig. 2 we also show the dependence of the dispersion curves on variations in $\hat{B}$ and $\hat{C}_w$. These curves exhibit a range of wave numbers for which $\lambda_r>0$ indicating a linear instability, and possess well-defined most dangerous and cutoff modes. It is clearly seen in Fig. 2(a) that decreasing the relative significance of wall damping leads to an increase in the maximal growth rate and a shift of the wave numbers associated with the most dangerous and cutoff modes to larger values. We also show an example wherein decreasing the magnitude of the wall tension is destabilizing; this is depicted in Fig. 2(b), which was generated with $\hat{B}=1$.

In the $k\to 0$ limit, substitution of the following regular perturbation expansion for the growth rate $\lambda\sim\lambda_0+k\lambda_1+k^2\lambda_2+O(k^3)$ and solution of the resultant sequence of problems order-by-order in powers of k yields two branches, which are described by

$$\lambda \sim -2ik + \frac{8\,\mathrm{Re}}{15}\delta k^2 + O(k^3),$$

$$\lambda \sim -\frac{6i\delta}{\hat{B}}k - \frac{1}{\hat{B}}\left(\frac{1}{\hat{C}_w}+\frac{1}{\hat{C}}\right)k^2 + O(k^3). \tag{80}$$

These branches correspond to the familiar "hydrodynamic" mode and an additional "wall mode," which arises due to substrate flexibility. These results indicate that inertia is the destabilizing mechanism in the long-wave limit even in the presence of wall flexibility, which does not introduce a new unstable mode. The absence of wall effects from the hydrodynamic mode also explains why the dispersion curves shown in Figs. 2(a) and 2(b) are virtually indistinguishable in this limit.

We also perturb Eqs. (51) and (52) using the normal mode expansion provided by Eq. (78) to obtain

$$\lambda = \frac{(1+\beta)k^4(1+\beta-\beta k^2)+\alpha^2k^2(1-k^2)}{k^2(\beta+1)^2+\alpha^2} - i\frac{k(\alpha^2+(1+\beta)^2k^2-\alpha k^4)}{k^2(\beta+1)^2+\alpha^2}. \tag{81}$$

The marginal stability curve is obtained by setting $\lambda_r=0$ and this yields the following expression:

$$(1+\beta)k_c^2(1+\beta-\beta k_c^2)+\alpha^2(1-k_c^2)=0 \tag{82}$$

(note there is also a double root at $k=0$), which is shown in Fig. 3. It can be concluded from this figure that, for a given value of β, the ratio of wall to surface tension, k_c decreases with α, the modified wall damping parameter. A similar behavior to that shown in Fig. 2 is also seen in Fig. 3: for sufficiently small wall damping, decreasing the wall tension is highly destabilizing, while for $\alpha\approx 3.7$, this trend is re-

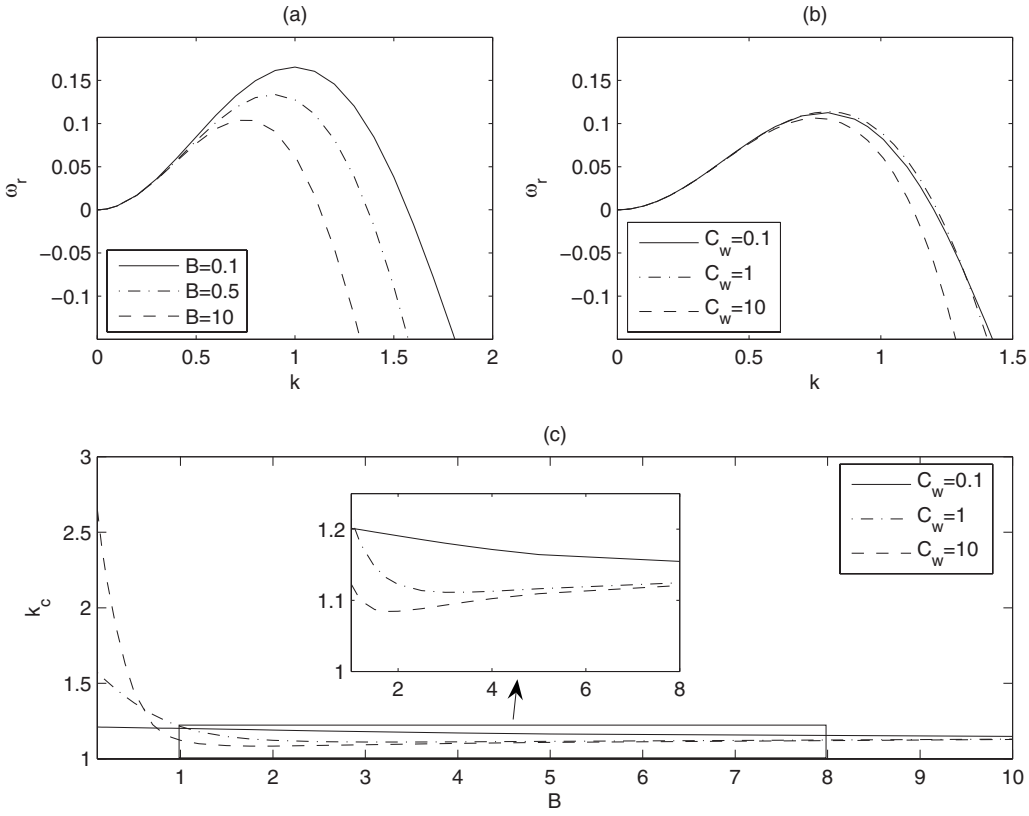

FIG. 4. Dispersion curves showing the effect of varying $\hat{B}$ (a) and $\hat{C}_w$ (b) on the linear stability of the falling film; (c) marginal stability curve. Unless stated otherwise in the legends, $\hat{B}=\widehat{\mathrm{Re}}=\widehat{We}=\hat{C}=\hat{C}_w=1$.

versed (see inset in Fig. 3). Examples of dispersion curves where decreasing wall damping and tension is destabilizing are also shown in Fig. 3.

In the $k\to 0$ limit, substitution of the following regular perturbation expansion for the real part of the growth rate $\lambda_r\sim\lambda_{r0}+k\lambda_{r1}+k^2\lambda_{r2}+O(k^3)$ and the solution of the resultant sequence of problems order-by-order in powers of k yields $\lambda_r\sim k^2+O(k^3)$. This result shows, once again, that wall flexibility does not affect the linear stability of the system in the long-wave limit.

B. Integral theory

We perturb Eqs. (63), (65), and (67) about the steady state $(\eta,h,q)=(0,1,2/3)$ (and $\Delta P=0$):

$$(\eta,h,q)=(0,1,2/3)+(\hat{\eta},\hat{h},\hat{q})e^{ikx}e^{\lambda t}. \tag{83}$$

Substitution of this normal mode decomposition into Eqs. (63), (65), and (67) and subsequent linearization yields the following characteristic equation for λ:

$$\alpha_1+\alpha_2\left(\hat{B}\lambda+\frac{k^2}{\hat{C}_w}\right)+\frac{i}{k}(\lambda+\alpha_3)\left[\alpha_4+\left(\hat{B}\lambda+\frac{k^2}{\hat{C}_w}\right)\times\left(\lambda+\frac{k^2}{\hat{B}\hat{C}}\right)\right]=0, \tag{84}$$

where $\alpha_i(i=1,\ldots,4)$ are given by

$$\alpha_1\equiv-\frac{k^2\,\widehat{\mathrm{Re}}}{\widehat{We}}\left(\frac{6}{5}iq_0^2k+2\frac{2(1+3q_0)}{\widehat{\mathrm{Re}}}\right), \tag{85}$$

$$\alpha_2\equiv-\left(\frac{6}{5}iq_0^2k+\frac{2}{\widehat{\mathrm{Re}}}(1+3q_0)-i\frac{k^3}{\widehat{We}}\right), \tag{86}$$

$$\alpha_3\equiv\frac{12}{5}iq_0k+\frac{3}{\widehat{\mathrm{Re}}},\quad \alpha_4\equiv-\frac{\widehat{\mathrm{Re}}}{\widehat{We}\hat{B}\hat{C}_w}k^4, \tag{87}$$

wherein $q_0=2/3$. In order to determine the marginal stability curve, we set $\lambda_r=0$ and separate the real and imaginary components of Eq. (84):

$$\alpha_{1r}+\alpha_{2r}\frac{k_c^2}{\hat{C}_w}-\alpha_{2i}\hat{B}\lambda_i-\frac{1}{k_c}\left(\alpha_4-\hat{B}\lambda_i^2+\frac{k_c^4}{\hat{B}\hat{C}\hat{C}_w}\right)(\lambda_i+\alpha_{3i})-\alpha_{3r}\left(\frac{1}{\hat{C}}+\frac{1}{\hat{C}_w}\right)\lambda_ik_c=0, \tag{88}$$

$$\alpha_{1i}+\alpha_{2r}\hat{B}\lambda_i+\alpha_{2i}\frac{k_c^2}{\hat{C}_w}-\left(\frac{1}{\hat{C}}+\frac{1}{\hat{C}_w}\right)(\lambda_i^2+\alpha_{3i}\lambda_i)-\frac{\alpha_{3r}}{k_c}\hat{B}\lambda_i^2=0. \tag{89}$$

Solution of this equation for λ_i and substitution of the result into Eq. (88) yields a marginal stability curve, which relates k_c to the relevant dimensionless parameters. This is shown in Fig. 4. In the limit $\hat{B}\to\infty$, this reduces to the particularly simple relationship $k_c=\sqrt{4\widehat{\mathrm{We}}/3}$. Figure 4 shares qualitatively similar features with Figs. 2 and 3: wall flexibility, characterized by weak damping and tension is destabilizing and, with increasing damping, decreasing wall tension is stabilizing. The switch-over in the calculated trend occurs at

lower wall damping rates in the present case and the marginal stability curves associated with low wall tension also exhibit more pronounced minima than was seen in Fig. 2.

We have also examined the $k \to 0$ limit. Substitution of the regular perturbation expansion $\lambda \sim \lambda_0 + k\lambda_1 + k^2\lambda_2 + O(k^3)$ into Eq. (84) and solving the sequence of problems order-by-order in powers of k yields the following two branches:

$$\lambda \sim -2ik + \frac{4}{9}\widehat{\mathrm{Re}}\,k^2 + O(k^3),$$

$$\lambda \sim -\frac{1}{\hat{B}}\left(\frac{1}{\hat{C}_w} + \frac{1}{\hat{C}}\right)k^2 + O(k^3). \tag{90}$$

Inspection of the first asymptotic relation for λ shows the falling film is destabilized by inertia while from the second relation it can be seen that $\lambda < 0$. These results are also in line with those obtained from long-wave theory. The results of our transient numerical simulations are presented next.

IV. NUMERICAL RESULTS

A. Numerical procedures

We begin this section by briefly describing the numerical procedures employed in carrying out the computations. In order to solve both sets of equations (46), (47), (63), (65), and (67) we have used two numerical routines. One of these uses centered finite-differences to approximate spatial derivatives with one-sided differences at the boundaries, and the other employs finite-element discretization in space; both routines use Gear's method to advance the solution in time. The predictions of these two procedures are in excellent agreement. Numerical solutions are obtained starting from the following initial condition for h:

$$(h,H)(x,0) = 1 + 0.01 \times \exp(-5[x-5]^2), \quad \eta(x,0) = 0, \tag{91}$$

when solving Eqs. (46) and (47), that is, a small perturbation from the base state. Equations (91) are supplemented with $q(x,0) = 2/3$ when solving Eqs. (63), (65), and (67). The Gaussian term in $h(x,0)$ represents a small disturbance to the film surface which is required to initiate the dynamic evolution of the flow. The solutions obtained are subject to the following boundary conditions:

$$(h,H)(0,t) = 1, \quad \eta(0,t) = 0, \quad q(0,t) = \frac{2}{3},$$

$$(h,H)(L,t) = 1, \quad \eta(L,t) = 0, \quad q(L,t) = \frac{2}{3}; \tag{92}$$

where L represents the length of the computational domain. Up to 4000 and 20 000 grid points were utilized when the finite-element and finite-difference procedures were employed, respectively; convergence was achieved upon refinement of the spatial mesh.

In order to investigate the system dynamics in the weakly nonlinear regime, we follow the approach of Tseluiko and Papageorgiou [44] and rescale Eqs. (51) and (52) as follows: $x \to (L/\pi)x$, $t \to (L/\pi)^2 t$, $(d,H,\eta) \to (\pi/L)(d,H,\eta)$; this, then, leads to

$$d_t + dd_x + d_{xx} + \nu H_{xxxx} = 0, \tag{93}$$

$$\bar{\alpha}\eta_x + \beta\eta_{xx} - H_{xx} = 0, \tag{94}$$

where $\nu \equiv (\pi/L)^2$ and $\bar{\alpha} \equiv \alpha L/\pi$. Periodic solutions of the weakly nonlinear equations given by Eqs. (51) and (52) starting from

$$H(x,0) = 0.02 \times \cos(x), \quad \eta(x,0) = 0, \tag{95}$$

and subject to $H(0,t) = H(2\pi,t)$ and $\eta(0,t) = \eta(2\pi,t)$ in $x \in (0,2\pi)$ are found numerically. The equations are well suited to solutions using spectral methods, and bespoke methods of dealing with the linear, high-order terms [68] are of current interest; we adjust their algorithm to incorporate the additional terms due to substrate flexibility. Cross-checking was done via computations carried out using MATHEMATICA and solutions were obtained for $0.03 \le \nu \le 1.5$, $0.1 \le \bar{\alpha} \le 10$, and $0.1 \le \beta \le 10$. Our numerical results are described next.

B. Re=O(1): Weakly nonlinear dynamics

We begin the presentation of our results by examining briefly the film dynamics in the weakly nonlinear regime; this is described by Eqs. (93) and (94). In Figs. 5 and 6, we show the effect of varying ν on the solutions for H for the case of a rigid support, that is, with $\bar{\alpha} \to \infty$; the equations solved then reduce to the well-known Kuramoto-Sivashinsky equation. In Fig. 5, the panels depict $E = \int_0^{2\pi} H^2 dx$, the L^2 norm of the solution and a measure of the disturbance "energy," and space-time plots of H, respectively. As shown in these plots, varying the value of ν has a profound effect on the dynamics (see, for instance, the recent work of Tseluiko and Papageorgiou [44] and numerous references therein).

Increasing the length of the film by decreasing ν gives rise to bifurcations to a stable single mode steady state, single mode steady traveling waves and periodic homoclinic "bursts" [44] followed by a two-mode steady-state; these are shown in panels (a),(d); (b),(e); and (c),(f) of Fig. 5. Upon decreasing the value of ν further, we observe homoclinic bursts for $\nu = 0.09$, which appear to be chaotic [see Figs. 6(a) and 6(d)], a multimodal attracting solution for $\nu = 0.07$ [see Figs. 6(b) and 6(e)], and chaotic solutions for $\nu = 0.03$ [see Figs. 6(c) and 6(f)]. We have also found that for sufficiently large ν that correspond to short films, the amplitude of the disturbance applied decays; this case is not shown. We now consider how substrate flexibility affects the trends observed in the rigid wall case.

In Fig. 7, we show the effect of varying $\bar{\alpha}$ and β on the space-time plots of H and E_1, the L^2 norm of the solutions for H; the results for η mirror these and are not shown. We start by considering the $\nu = 0.2$ case for which periodic homoclinic bursts are observed in the rigid wall case [see Figs. 5(c) and 5(f)]. A transition from chaotic oscillations to time-periodic attracting solutions follows the increase of $\bar{\alpha}$ from

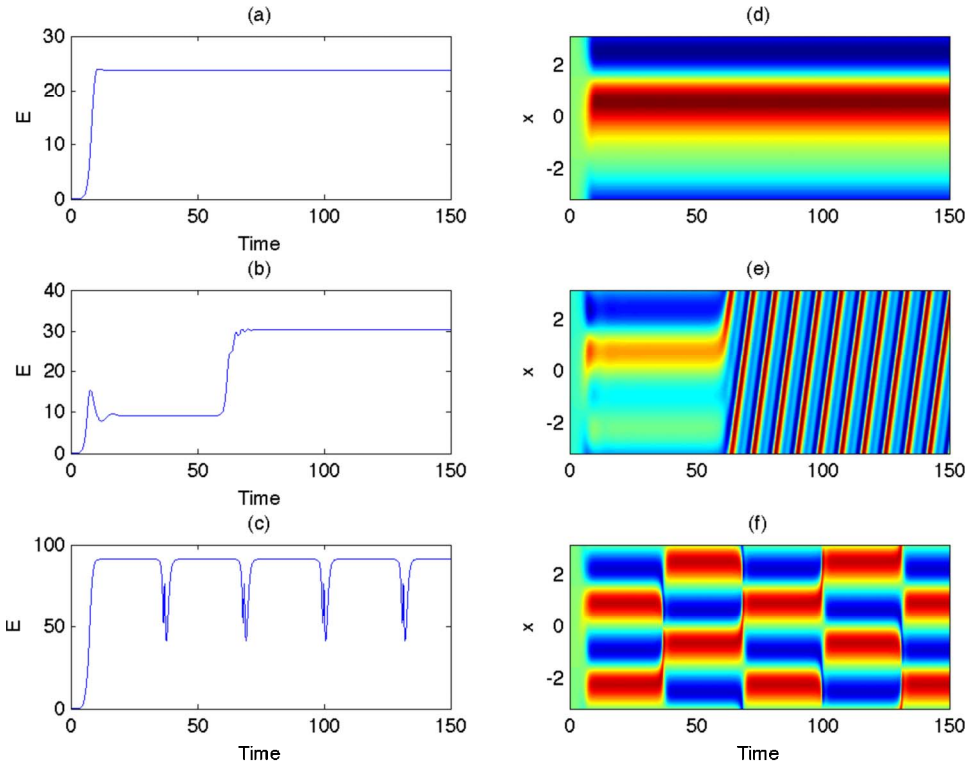

FIG. 5. (Color online) Numerical results for the KS equation $E(t)$ $\nu=0.4,0.27,0.2$ (a)–(c), respectively, and corresponding space time plots showing the evolving structure in (d)—(f).

0.1 to 10. Increasing β from 0.2 to 10 results in a transition from chaotic solutions to two-mode solutions separated by periodic homoclinic bursts. The dynamics observed in the large β case are therefore rather similar to those observed in the rigid wall case; decreasing the values of β (and $\bar{\alpha}$) leads to departures from this case and a lowering of the critical conditions for the onset of chaos; similar trends were observed at higher ν values.

We next decrease the value of ν to $\nu=0.07$. In the rigid wall case, one would expect there to be a three-mode attractor preceded by transient oscillations [see Figs. 6(b) and 6(e)]. As shown in Fig. 8, increasing $\bar{\alpha}$ from 0.1 to 10 results in a transition from chaotic to long two-mode traveling wave solutions; increasing β from 0.2 to 10 gives rise to a transition from chaotic to three-mode steady-states preceded by transient oscillations, which resemble the solutions obtained

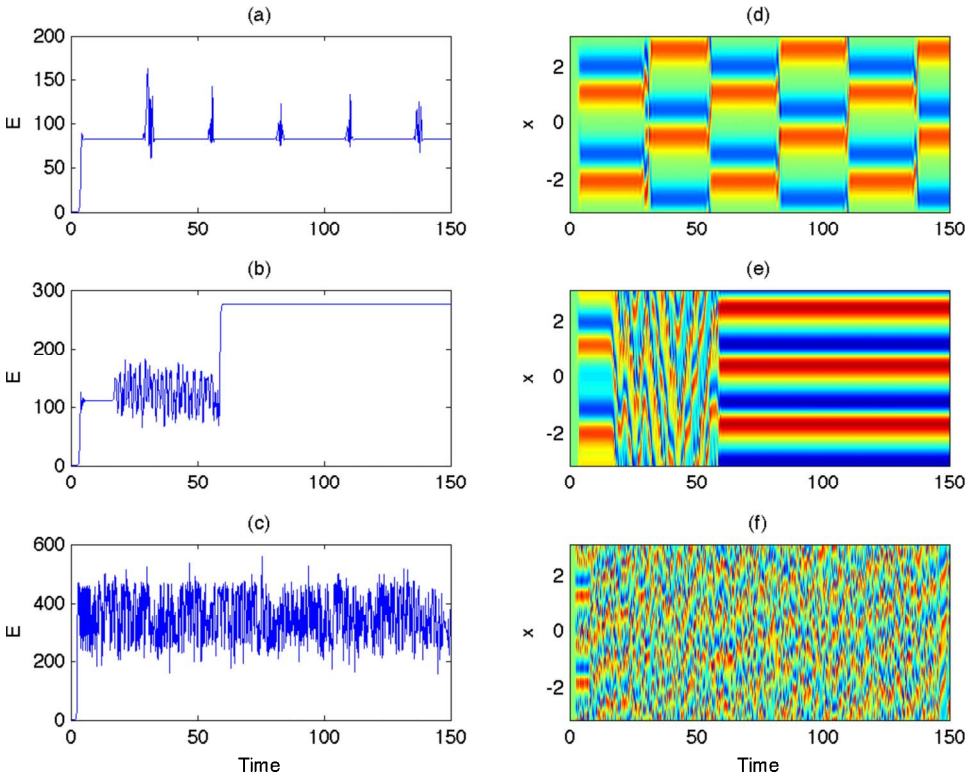

FIG. 6. (Color online) Numerical results for the KS equation $E(t)$ for $\nu=0.09,0.07,0.03$ (a)–(c), respectively, and corresponding space time plots showing the evolving structure in (d)—(f).

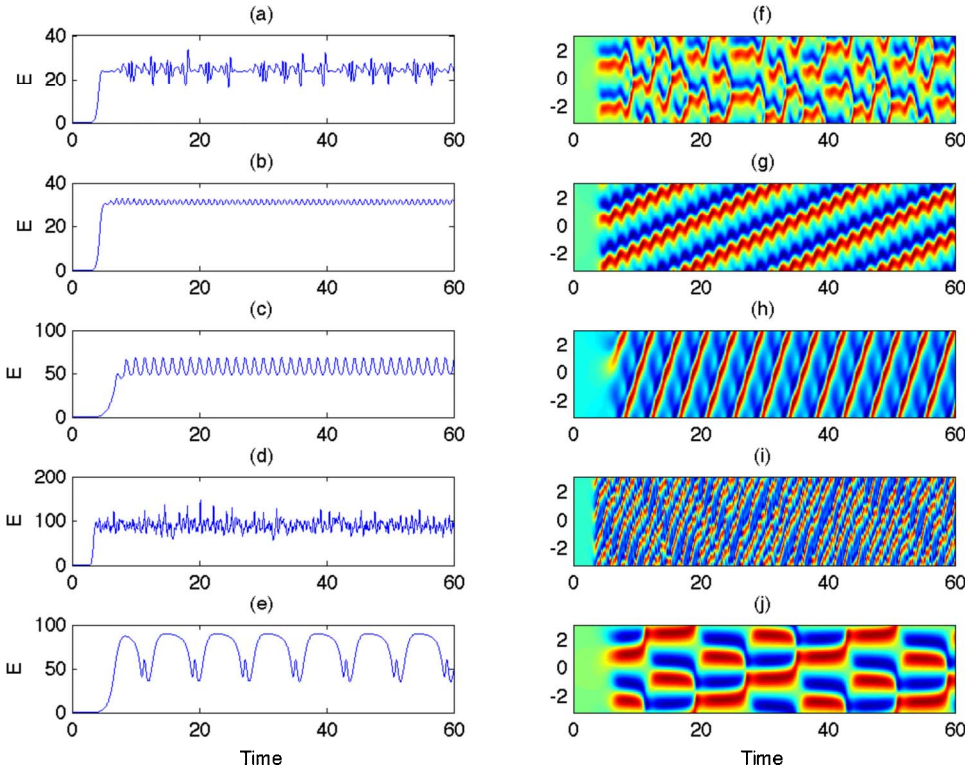

FIG. 7. (Color online) Numerical results for Eqs. (51) and (52): $E_h(t)$ and space-time plots for $\nu=0.2$ and $(\bar{\alpha},\beta)=(0.1,1),(1,1),(10,1),(1,0.2),(1,10)$ shown in (a)—(e) and (f)—(j).

in the rigid case. It is clearly seen that decreasing the value of $\bar{\alpha}$ and β promote chaotic oscillations.

The above trends can be rationalized by considering Eqs. (93) and (94) for $\bar{\alpha}\ll 1$ and $\beta=O(1)$. This limiting case can be described by Eqs. (69) and (70), which, following the rescaling, $x\to(L/\pi)x$, $t\to(L/\pi)^2 t$, $(d,H,\eta)\to(\pi/L)(d,H,\eta)$, reads

$$\hat{\beta}H_t+\hat{\beta}^2HH_x-\nu^{-1/2}\hat{\beta}(\hat{\beta}-1)H_x+\hat{\beta}H_{xx}+\nu H_{xxxx}=0. \tag{96}$$

Multiplication of this equation over x from 0 to 2π and making use of periodicity (with period 2π) yields

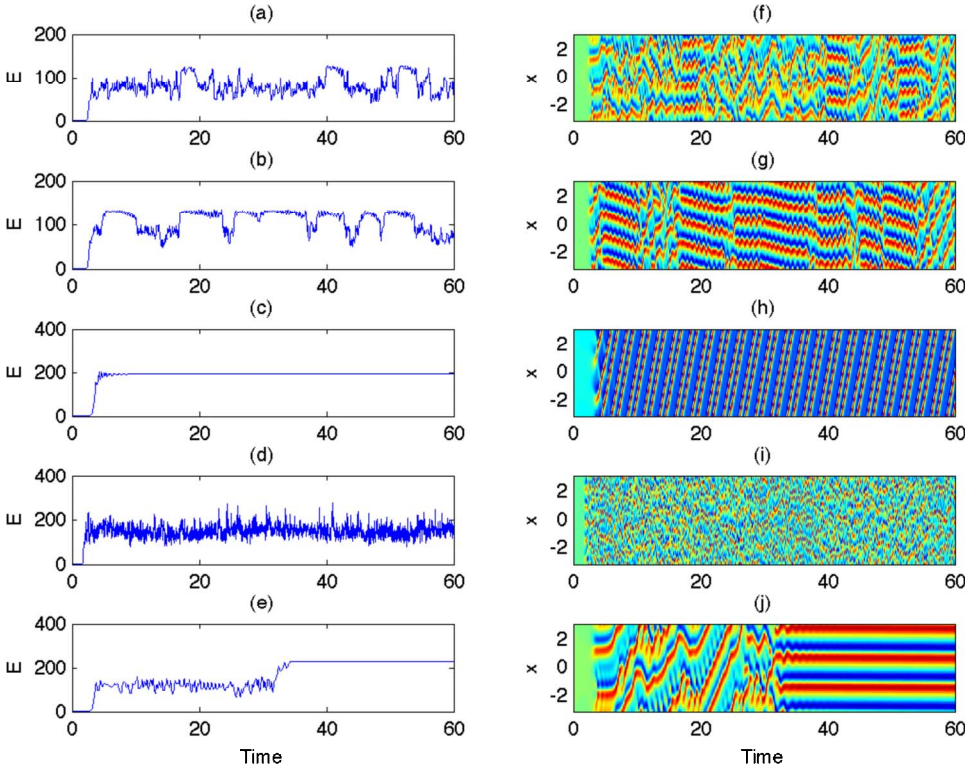

FIG. 8. (Color online) Numerical results for Eqs. (51) and (52): $E_h(t)$ and space-time plots for $\nu=0.07$ and $(\bar{\alpha},\beta)=(0.1,1),(1,1),(10,1),(1,0.2),(1,10)$ shown in (a)—(e) and (f)—(j).

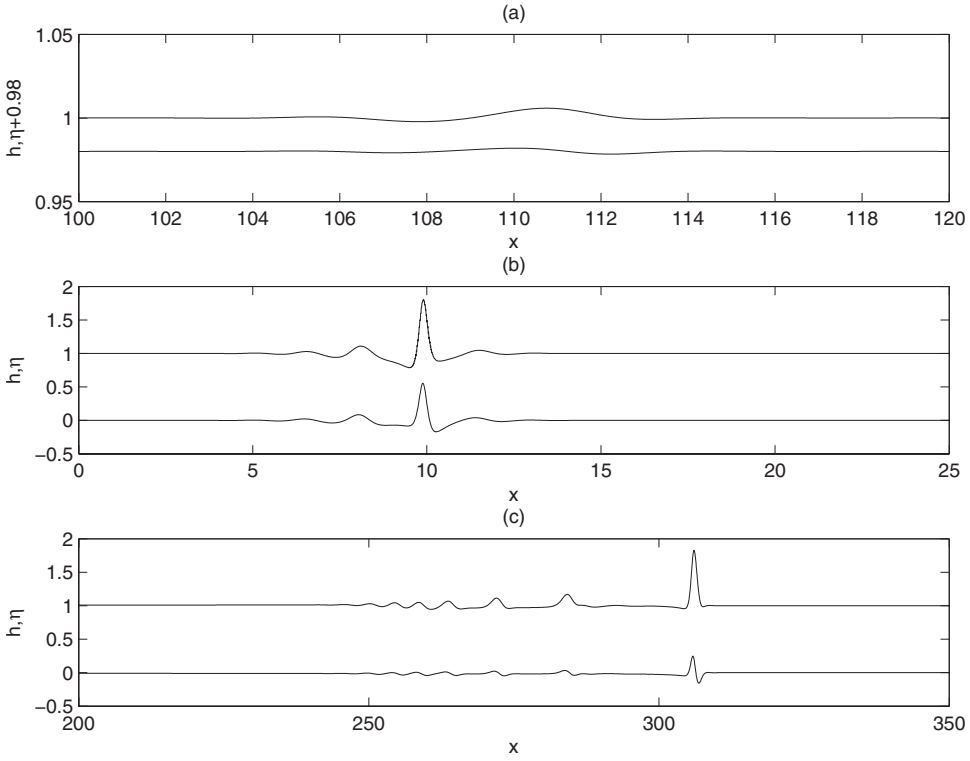

FIG. 9. Numerical solutions of Eqs. (46) and (47). (a) $\delta=0.05$, $\mathrm{Re}=\hat{B}=\hat{C}=\hat{C}_w=1$, $t=70$; (b) $\delta=0.05$, $\mathrm{Re}=10$, $\hat{B}=\hat{C}=\hat{C}_w=1$, $t=2.5$; (c) $\delta=0.2$, $\mathrm{Re}=\hat{B}=\hat{C}=\hat{C}_w=1$, $t=140$.

$$\frac{1}{2}\frac{d}{dt}\int_0^{2\pi} H^2 dx = \int_0^{2\pi} H_x^2 dx - \frac{\nu}{\hat{\beta}}\int_0^{2\pi} H_{xx}^2 dx. \qquad (97)$$

The first and second terms on the left-hand side of Eq. (97), which are related to the nonlinearity and the capillary term in Eq. (93), are destabilizing and stabilizing, respectively. In the rigid substrate case, that is, for $\beta \gg 1$ so $\hat{\beta} \sim 1$, decreasing ν leads to the occurrence of chaotic solutions, as shown in Figs. 6(c) and 6(f). Inspection of Eq. (97) reveals that decreasing β decreases the value of the coefficient of the stabilizing term $\nu/\hat{\beta}$; this promotes the transition to chaos. We speculate that a similar mechanism must hold with respect to wall tension to the extent that lowering the wall tension also increases the wall deformation. We turn our attention now to examining the flow at $\mathrm{Re}=O(1)$.

C. Re=O(1): Modified Benney dynamics

Here, we provide a brief discussion of the numerical results obtained via the solution of Eqs. (46) and (47). We show in Fig. 9 the effect of varying δ and Re on the film and wall dynamics with $\hat{B}=\hat{C}=\hat{C}_w=1$. For $\delta=0.05$ and $\mathrm{Re}=1$, it is seen that the flow is accompanied by mild deformations, characterized by waves in both the film and underlying substrate, which are of small amplitude [see Fig. 9(a)]. Increasing the value of δ and/or Re gives rise to large-amplitude wave formation, as shown in Figs. 9(b) and 9(c). This is to be expected since increasing δ and Re corresponds to an increase in the inertial contribution. For the values of δ and Re used to generate the results shown in Figs. 9(b) and 9(c), the simulations were halted due to finite-time "blow-up," which is a feature of equations that are of the Benney type.

In Fig. 10, we present the results of investigating the effect of varying $\hat{B}$ and $\hat{C}_w$ on the dynamics. For relatively low damping rates, characterized by $\hat{B}=0.1$, the flexible substrate undergoes substantial deformation, which appears to be similar in magnitude to the large-amplitude waves exhibited by the film, as shown in Fig. 10. This result can be explained by considering Eqs. (46) and (47) in the limit of small $\hat{B}$ and δ: Eq. (47) reduces to $-(\hat{C}/\hat{C}_w)\eta_{\xi\xi}+H_{\xi\xi}\approx 0$. Solution of this equation subject to Eqs. (92) and starting from $\eta(\xi,0)=0$ and $H(\xi,0)\approx 1$, yields $\eta\approx(\hat{C}_w/\hat{C})(h-1)$.

Increasing the value of $\hat{B}$ from 0.1 to 10, which corresponds to an increase in the wall damping rates, leads to very small wall deformations in relation to the wave amplitudes and recovers the rigid substrate case [see Figs. 10(b) and 10(c)]. Increasing the relative magnitude of wall tension by decreasing the value of $\hat{C}_w$ yields a similar result to increasing $\hat{B}$ and also recovers the rigid wall case. In contrast, a decrease in $\hat{C}_w$ has a drastic effect on the dynamics, leading to the formation of large-amplitude waves in the substrate and the possibility that the air-liquid and solid-liquid interfaces can come into contact in finite time; this is shown in Fig. 10(e). In summary, decreasing the magnitude of wall damping renders the substrate enslaved to the film dynamics and $\eta\approx(\hat{C}_w/\hat{C})(h-1)$, while decreasing the wall tension leads to large wall deformations which occur sufficiently rapidly for the wall to come into contact with the air-liquid interface; increasing $\hat{B}$ and/or $\hat{C}_w$ recovers the rigid wall case.

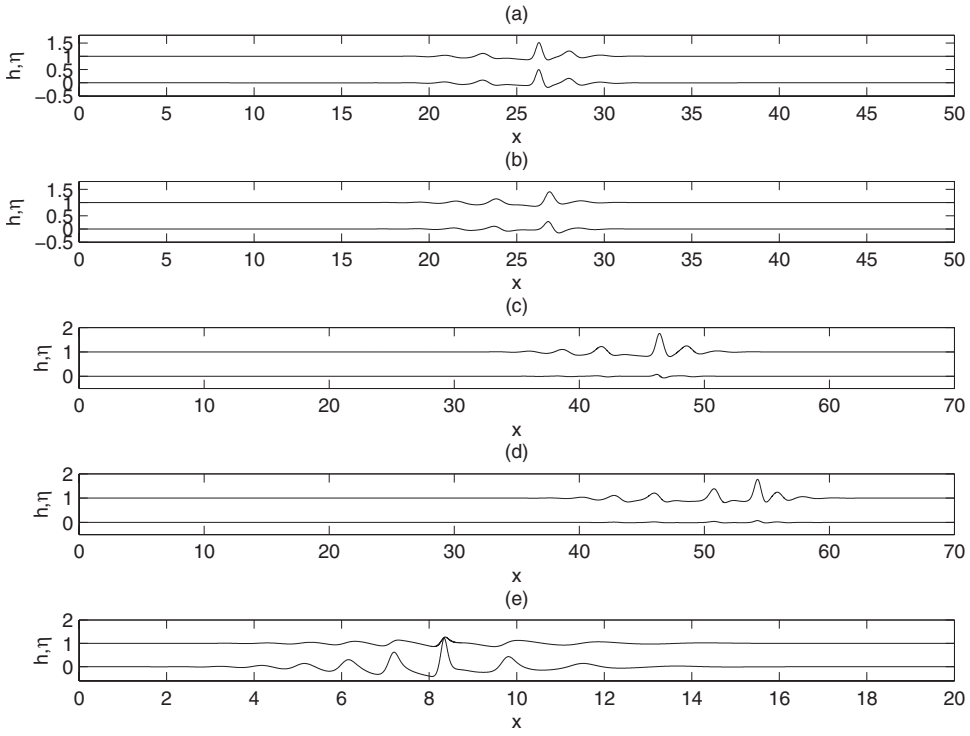

FIG. 10. Numerical solutions of Eqs. (46) and (47). (a) $\hat{B}=0.1$, $\hat{C}_w=1$, $t=10.2$; (b) $\hat{B}=\hat{C}_w=1$, $t=10.8$; (c) $\hat{B}=10$, $\hat{C}_w=1$, $t=20$; (d) $\hat{B}=1$, $\hat{C}_w=0.1$, $t=22$; (e) $\hat{B}=1$, $\hat{C}_w=10$, $t=4.92$; the rest of the parameter values are $\delta=0.05$, Re=5, and $\hat{C}=1$.

D. Evolution at Re=$O(\delta^{-1})$

Here, we present a discussion of the numerical solutions of Eqs. (63), (65), and (67), which allow us to explore the effects of wall flexibility on the system dynamics with significant inertial contributions. We begin by examining the spatiotemporal evolution of the film and substrate, shown in Fig. 11, with Re=3, $\hat{C}=0.3$, $\hat{B}=\hat{C}_w=1$; only the case of $p_g=p_w$ is considered in the present work and $\Delta p=0$ in the results presented below. At relatively early times, disturbances in η and h form a wave packet, which is convected away from the inlet, leaving behind a smooth, waveless region. At later times, large-amplitude waves begin to separate from this wave packet and propagate rapidly downstream, as shown in Figs. 11(a)–11(c). Close inspection of the structures shown in Fig. 11 reveals that severe depressions in the substrate deflection coincide with the down-slope regions of the large-amplitude waves in the film. The volumetric flow rate,

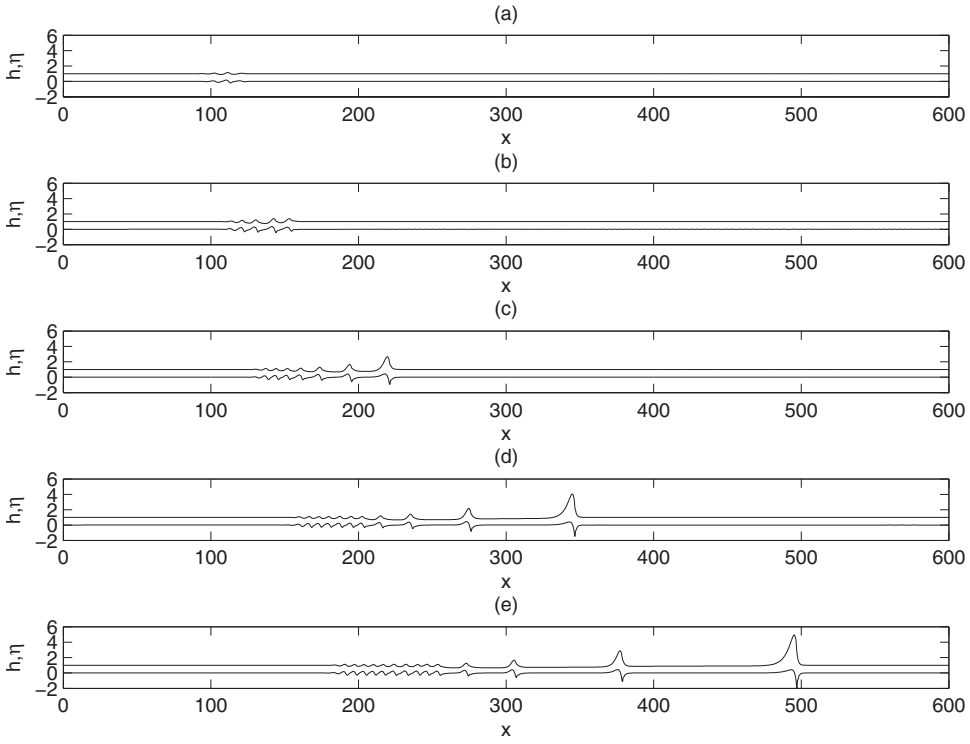

FIG. 11. Evolution of h and η obtained via numerical solution of Eqs. (63), (65), and (67) with Re=3, $\hat{C}=0.3$, $\hat{B}=\hat{C}_w=1$; the solutions are shown at $t=50,70,100,140,180$ in panels (a)–(e), respectively.

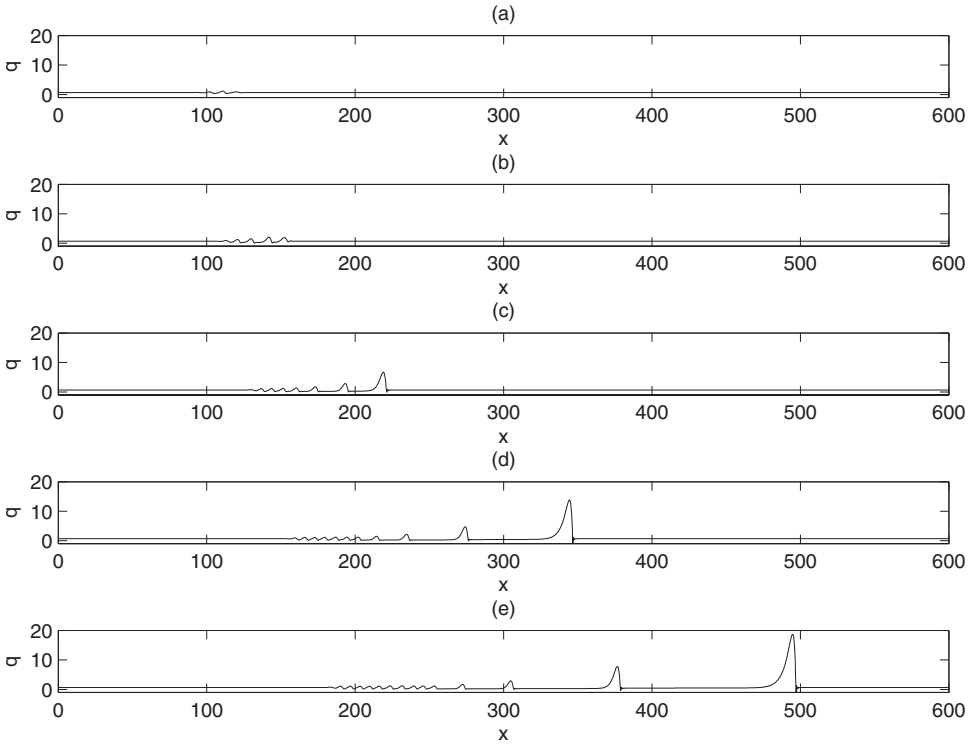

FIG. 12. Evolution of q obtained via numerical solution of Eqs. (63), (65), and (67) for the same parameters as in Fig. 11.

q, also exhibits large-amplitude wave structures, which coincide with those of the film, as illustrated in Fig. 12. In contrast to the results presented in Sec. IV C, finite-time "blow-up" was not observed in any of the simulations carried out via solution of Eqs. (63), (65), and (67) in the present work.

In Fig. 13, we show the effect of varying $\hat{B}$ on the numerical solutions. Decreasing the value of $\hat{B}$ leads to severe deformations in the substrate, characterized by large deflections [see Fig. 13(a)]. Positive and negative deflections are spatially coincident with upwards and downwards sloping regions of the wavy film, respectively, and the distance between the air-liquid and liquid-solid interfaces at the peak of the substrate deflection decreases considerably during the course of the simulation; this is qualitatively similar to the

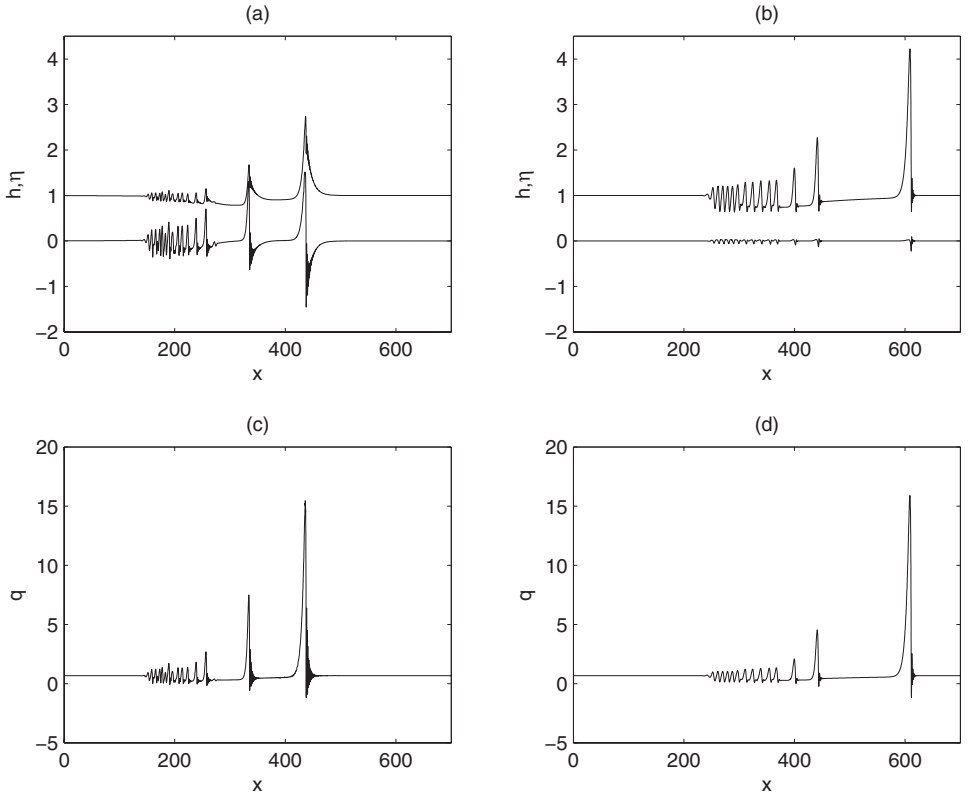

FIG. 13. The effect of varying $\hat{B}$ on the numerical solutions of Eqs. (63), (65), and (67): $\hat{B}=0.1$, $t=127.63$, and $\hat{B}=10$, $t=219.86$ in panels (a), (c) and (b), (d), respectively; the rest of the parameters remain the same as in Fig. 11.

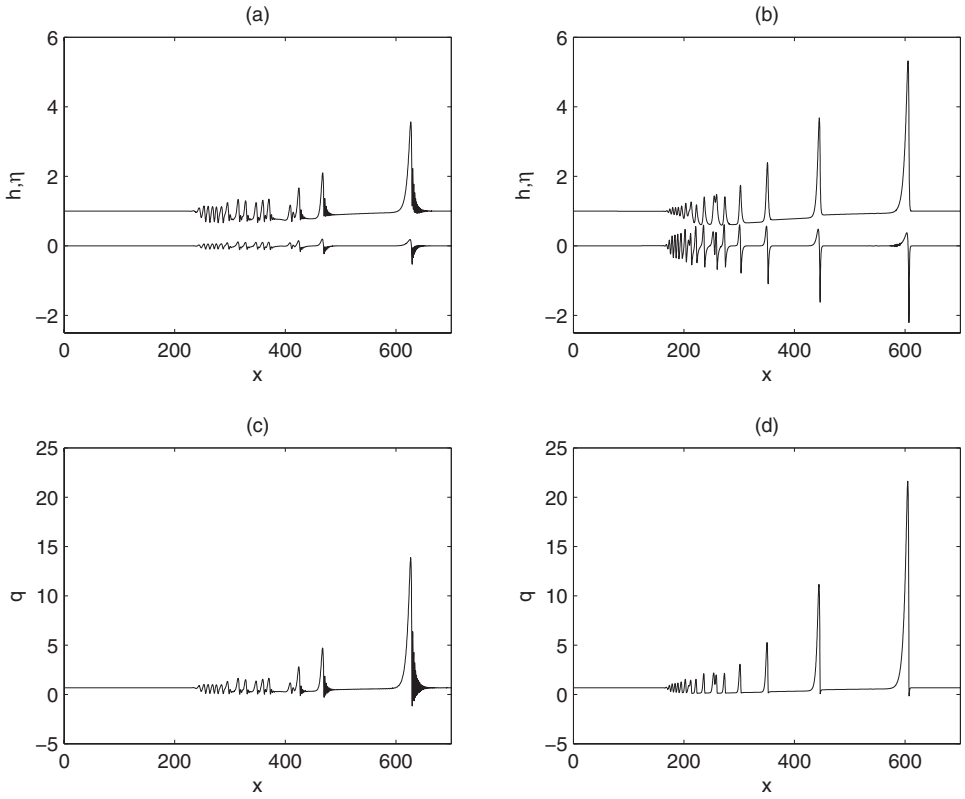

FIG. 14. The effect of varying $\hat{C}_w$ on the numerical solutions of Eqs. (63), (65), and (67): $\hat{C}_w=0.1$, $t=157.67$ and $\hat{C}_w=10$, $t=181.28$ in panels (a), (c) and (b), (d), respectively; the rest of the parameters remain the same as in Fig. 11.

results shown in Fig. 10(e) obtained by solving the modified Benney equations, (46) and (47), in the case of weak wall tension. Increasing the relative magnitude of wall damping via an increase in $\hat{B}$, results in very small-amplitude substrate deflections and the formation of solitary waves in the film preceded by capillary ripples [see Fig. 13(b)]; similar results to those shown in Figs. 13(b) and 13(d) have also been reported in studies of falling films on rigid substrates [3]. The structures exhibited by q remain qualitatively insensitive to changes in $\hat{B}$.

In Fig. 14, it is clearly seen that a decrease in $\hat{C}_w$ leads to similar results to those associated with large $\hat{B}$ values, while decreasing wall tension by increasing $\hat{C}_w$, on the other hand, gives rise to large substrate deformations. A comparison of Figs. 13(a) and 14(b) reveals that the waves in both the film and substrate in the case of weak wall tension travel faster and are more pulselike and separated by relatively long, flat regions than in the weak damping case; in the latter case, the waves are slower, more spread out and have lower maximal amplitudes.

V. CONCLUDING REMARKS

We have studied the dynamics of falling films on flexible inclines and developed evolution equations for the film thickness and substrate deflection using long-wave theory and the integral method for low and moderate Reynolds numbers, respectively. By systematic investigation of these equations using linear theory and numerical simulations we can see that the weakly nonlinear equations indicate that decreasing the relative magnitude of substrate tension and/or the rate of its damping leads to severe deformation of the substrate and promotes the development of chaotic solutions, which are a feature of these equations in the rigid substrate case for sufficiently long films. Solution of the modified Benney and Shkadov equations reveals that increasing the degree of wall flexibility can lead to situations in which the air-liquid and liquid-solid interfaces can touch due to severe substrate deformations. The destabilization produced by lowering the wall damping and tension are apparently caused by an effective weakening of the stabilizing capillary forces at the air-liquid interface. From a practical perspective, the results of this work may be useful for designing flexible surfaces to promote interfacial instabilities, which would then lead to improvements in heat/mass transport and mixing. We have used the simplest model of a flexible substrate and it would now also be of interest to consider other types of models for the wall in order to explore the possibility of using flexible walls to inhibit interfacial instabilities [69,70].

ACKNOWLEDGMENTS

O.K.M. acknowledges support from EPSRC and DTI through Grant Nos. EP/D503051/1, EP/D503051/1, and TP//ZEE/6/1/21191. Acknowledgment is also made to the Donors of the The American Chemical Society Petroleum Research Fund for partial support of this research (S.K.). R.V.C. thanks the Departments of Mathematics at the University of Alberta and University of British Columbia for their hospitality whilst this work was carried out.

[1] A. Oron, S. H. Davis, and S. G. Bankoff, Rev. Mod. Phys. **69**, 931 (1997).
[2] R. V. Craster and O. K. Matar (unpublished).
[3] H.-C. Chang and E. A. Demekhin, *Complex Wave Dynamics on Thin Films* (Elsevier, Amsterdam, 2002).
[4] P. L. Kapitza, J. Exp. Theor. Phys. **18**, 3 (1948).
[5] P. L. Kapitza and S. P. Kapitza, J. Exp. Theor. Phys. **19**, 105 (1949).
[6] S. V. Alekseenko, V. E. Nakoryakov, and B. T. Pokusaev, *Wave Flow of Liquid Films* (Begel House, New York, 1994).
[7] J. Liu and J. P. Gollub, Phys. Rev. Lett. **70**, 2289 (1993).
[8] J. Liu and J. P. Gollub, Phys. Fluids **6**, 1702 (1994).
[9] J. Liu, J. B. Schneider, and J. P. Gollub, Phys. Fluids **7**, 55 (1995).
[10] T. Nosoko, P. N. Yoshimura, T. Nagata, and L. Okawa, Chem. Eng. Sci. **51**, 725 (1996).
[11] C. D. Park and T. Nosoko, AIChE J. **49**, 2715 (2003).
[12] T. Nosoko and A. Miyara, Phys. Fluids **16**, 1118 (2004).
[13] M. Vlachogiannis and V. Bontozoglou, J. Fluid Mech. **435**, 191 (2001).
[14] K. Argyriadi, K. Serifi, and V. Bontozoglou, Phys. Fluids **16**, 2457 (2004).
[15] C. S. Yih, in *Proceedings of the 2nd US Congress on Applied Mechanics* (ASME, New York, 1955), pp. 623–628.
[16] C. S. Yih, Phys. Fluids **6**, 321 (1963).
[17] T. B. Benjamin, J. Fluid Mech. **2**, 554 (1957).
[18] D. J. Benney, J. Math. Phys. **45**, 150 (1966).
[19] S. P. Lin, J. Fluid Mech. **36**, 113 (1969).
[20] B. Gjevik, Phys. Fluids **13**, 1918 (1970).
[21] G. J. Roskes, Phys. Fluids **13**, 1440 (1970).
[22] R. W. Atherton and G. M. Homsy, Chem. Eng. Commun. **2**, 57 (1976).
[23] A. Pumir, P. Manneville, and Y. Pomeau, J. Fluid Mech. **135**, 27 (1983).
[24] C. Nakaya, Phys. Fluids A **1**, 1143 (1989).
[25] S. W. Joo and S. H. Davis, J. Fluid Mech. **242**, 529 (1992).
[26] H.-C. Chang, Annu. Rev. Fluid Mech. **26**, 103 (1994).
[27] C.-H. Chang and E. I. Frances, Colloids Surf., A **100**, 1 (1995).
[28] H. Chang and E. A. Demekhin, J. Fluid Mech. **380**, 233 (1999).
[29] T. Ooshida, Phys. Fluids **11**, 3247 (1999).
[30] C. Ruyer-Quil and P. Manneville, Eur. Phys. J. B **6**, 277 (1998).
[31] C. Ruyer-Quil and P. Manneville, Eur. Phys. J. B **15**, 357 (2000).
[32] B. Scheid, C. Ruyer-Quil, U. Thiele, O. Kabov, J. Legros, and P. Colinet, J. Fluid Mech. **527**, 303 (2005).
[33] B. Scheid, C. Ruyer-Quil, and P. Manneville, J. Fluid Mech. **562**, 183 (2006).
[34] G. M. Homsy, Lect. Appl. Math. **15**, 191 (1974).
[35] A. A. Nepomnyashcy, Izv. Akad. Nauk, Mekh. Zhidk. Gaza **3**, 1143 (1974).
[36] Y. Kuramoto and T. Tsuzuki, Prog. Theor. Phys. **54**, 687 (1975).
[37] Y. Kuramoto and T. Tsuzuki, Prog. Theor. Phys. **55**, 356 (1976).
[38] G. I. Sivashinsky, Acta Astron. **4**, 1175 (1977).
[39] G. I. Sivashinsky and D. M. Michelson, Prog. Theor. Phys. **63**, 2112 (1980).
[40] T. Shlang and G. I. Sivashinsky, J. Phys. (France) **43**, 459 (1982).
[41] A. P. Hooper and R. Grimshaw, Phys. Fluids **28**, 37 (1985).
[42] D. T. Papageorgiou, C. Maldarelli, and D. S. Rumschitzki, Phys. Fluids A **2**, 340 (1990).
[43] A. V. Coward, D. T. Papageorgiou, and Y. S. Smyrlis, Z. Angew. Math. Phys. **46**, 1 (1995).
[44] D. Tseluiko and D. T. Papageorgiou, J. Fluid Mech. **556**, 361 (2006).
[45] J. M. Hyman and B. Nikolaenko, Physica D **18**, 113 (1986).
[46] I. G. Kevrekidis, B. Nicolaenko, and J. C. Scovel, SIAM J. Appl. Math. **50**, 760 (1990).
[47] E. A. Demekhin, G. Y. Tokarev, and V. Y. Shkadov, Physica D **52**, 338 (1991).
[48] D. T. Papageogriou and Y. S. Smyrlis, Theor. Comput. Fluid Dyn. **3**, 15 (1991).
[49] Y. S. Smyrlis and D. T. Papageorgiou, Proc. Natl. Acad. Sci. U.S.A. **88**, 11129 (1991).
[50] Y. S. Smyrlis and D. T. Papageorgiou (unpublished).
[51] P. L. Kapitza (unpublished).
[52] V. Y. Shkadov, Fluid Dyn. **2**, 21 (1967).
[53] A. V. Bunov, E. A. Demekhin, and V. Y. Shkadov, J. Appl. Math. Mech. **48**, 691 (1984).
[54] G. M. Sisoev and V. Y. Shkadov, Fluid Dyn. **32**, 784 (1997).
[55] G. M. Sisoev and V. Y. Shkadov, Phys. Dokl. **42**, 683 (1997).
[56] V. Y. Shkadov and G. M. Sisoev, Fluid Dyn. Res. **35**, 357 (2004).
[57] J. J. Riley, M. Gad-el Hak, and R. W. Metcalfe, Annu. Rev. Fluid Mech. **20**, 393 (1988).
[58] J. B. Grotberg, Annu. Rev. Fluid Mech. **26**, 529 (1994).
[59] S. A. Berger and L.-D. Jou, Annu. Rev. Fluid Mech. **32**, 347 (2000).
[60] M. S. Carvalho and L. E. Scriven, J. Fluid Mech. **339**, 143 (1997).
[61] V. Kumaran and R. Muralikrishnan, Phys. Rev. Lett. **84**, 3310 (2000).
[62] O. K. Matar and S. Kumar, SIAM J. Appl. Math. **6**, 2144 (2004).
[63] O. K. Matar and S. Kumar, J. Eng. Math. **57**, 145 (2007).
[64] D. Halpern and J. B. Grotberg, J. Biomech. Eng. **115**, 271 (1993).
[65] D. Halpern and J. B. Grotberg, J. Fluid Mech. **244**, 615 (1992).
[66] L. D. Landau and E. M. Lifshitz, *Theory of Elasticity*, 3rd ed. (Butterworth-Heinemann, New York, 1986).
[67] H. B. Atabek and S. H. Lew, Biophys. J. **6**, 481 (1966).
[68] A.-K. Kassam and L. N. Trefethen, SIAM J. Sci. Comput. (USA) **26**, 1214 (2005).
[69] V. Gkanis and S. Kumar, Phys. Fluids **18**, 044103 (2006).
[70] Gaurav and V. Shankar, Phys. Fluids **19**, 024105 (2007).